Digital Domain Power Division Multiplexing Optical OFDM for Free Space Optical Communication (FSOC) Using 10-GHz Bandwidth Optical Components

Wahyu Hendra Gunawan [ID], Chi-Wai Chow [ID], *Senior Member, IEEE*, Yang Liu [ID], Yun-Han Chang [ID], Yin-He Jian, Ching-Wei Peng, and Chien-Hung Yeh [ID]

Abstract—We put forward and provide the first illustration of a high capacity and high spectral efficient free space optical communication (FSOC) system using digital domain power division multiplexing orthogonal-frequency-division-multiplexed (DDPD-O-OFDM) signal utilizing 10-GHz class optical components. In the proof-of-concept demonstration, a data rate of 2×30.8 Gbit/s can be achieved for each polarization multiplexed wavelength channel, fulfilling the pre-forward-error-correction bit-error-ratio (pre-FEC BER $= 3.8 \times 10^{-3}$). By employing the DDPD-O-OFDM here, the FSOC per channel capacity can be enhanced not only allowing the spectral overlapping of different orthogonal subcarriers, as in the case of OFDM; but also allowing channel multiplexing in the power domain to increase the spectral efficiency. The principle of DDPD-O-OFDM is discussed; and BER and signal-to-noise ratio (SNR) of different DDPD channels are experimentally measured.

Index Terms—Free space optical communication (FSOC), laser diode (LD), optical wireless communication (OWC), orthogonal frequency division multiplexing (OFDM).

I. INTRODUCTION

IN ORDER to satisfy the bandwidth demands of Internet-of-Things (IOT), cloud services, 4K/8K video streaming and online gaming, optical fiber access solutions, such as time division multiplexed (TDM) passive optical networks (PONs), wavelength division multiplexed (WDM) PONs [1]–[3], time-and-wavelength division multiplexed (TWDM) PON [4], orthogonal frequency division multiplexed PONs [5], [6], as well as coherent-PON [7] have been realized by providing enormous transmission capacity to users. Although the cost of optical fiber is low, underground installation is costly and time consuming. Digging ground to lay optical fibers is usually related to legal issues. Hence, the concept of combining fiber access and free-space optical communication (FSOC) has been extensively studied recently [8]–[10]. FSOC can provide high capacity, license-free, electromagnetic interference (EMI)-free, reliable and flexible optical transmission links [11], [12]. In some places, due to the geographical limitations, using FSOC to replace optical fibers can significantly reduce the deployment cost and complexity.

FSOC is regarded as a kind of optical wireless communication (OWC) [13], which makes use of all the available optical spectra, including ultra-violet (UV), visible-light and infra-red (IR) to carry data for transmission. The available communication spectrum is more than 2000 times of that in conventional radio-frequency (RF) communication [14]. OWC utilizing the visible light spectrum is known as visible light communication (VLC) [15]–[18]. FSOC is based on IR spectrum [19], the optical components, such as laser diodes (LDs), photodiodes (PDs), modulators, erbium-doped fiber amplifier (EDFA) optimized for the PON systems can be directly employed. To achieve high capacity FSOC, advanced modulations and multiplexing techniques can be utilized. Table I summaries different IR based FSOC systems and their performances. Modulation schemes, such as non-return-to-zero (NRZ) on-off-keying (OOK), return-to-zero (RZ) OOK, chirped RZ (CRZ) and carrier-suppressed RZ (CSRZ) can be employed [20]–[25]. In order to enhance the spectral efficiency, FSOC systems employing differential phase-shift-keying (DPSK) [26], dual-polarization quadrature-phase-shift-keying (DP-QPSK) [27], optical tandem sideband (OTSB) and optical single sideband (OSSB) orthogonal frequency division multiplexing (OFDM) [28] can be utilized to enhance the spectral efficiency. Although pulse-position-modulation (PPM) [29] is not spectral efficient, the pulse modulation is robust against inter-symbol interference (ISI) caused by multiple pathways or reflections in FSOC systems. Besides, combining PPM and minimum-shift-keying (MSK) can improve the bit-error-rate (BER) performance when compared with PSK and PPM

TABLE I
DIFFERENT IR BASED FSOC SYSTEMS

Ref.	Modulation	Data-rate	Distance	λ	Spectral efficiency (bit/s/Hz)	Sim./ Exp.
[20]	NRZ-OOK, RZ-OOK	5 Mbit/s	5.5 m	830 nm	0.067	Exp.
[20]	BPSK	50 kbit/s	5.5 m	830 nm	0.00067	Exp.
[21]	NRZ-OOK	4 × 1.25 Gbit/s	1.1 km	850 to 847.6 nm	0.125	Sim.
[22]	NRZ-OOK	1 Gbit/s	1.14 km	1550 nm	1	Exp.
[23]	NRZ-OOK	1 Gbit/s	5 km	850 nm	--	Sim.
[24]	NRZ-OOK	1.25 Gbit/s	104 m	1550nm	0.125	Exp.
[25]	RZ, CRZ, CSRZ	2.5 Gbit/s	>7 km	1550nm	--	Sim.
[26]	NRZ-DPSK	2.5 Gbit/s	300 km	1553.5 to 1548nm	1.33	Sim.
[27]	DP-QPSK	16 × 100 Gbit/s	80 m	1546 to 1558 nm	1.43	Exp.
[28]	OFDM-OTSB	5 Gbit/s	<6 km	1550 nm	0.67	Sim.
[28]	OFDM-OSSB	5 Gbit/s	6.2 km	1550 nm	0.67	Sim.
[29]	PPM	2.4 Gbit/s	0.1 km	1550 nm	--	Sim.
[30]	PPM-MSK	2 Gbit/s	1 km	850 nm	--	Sim.
[31]	OAM	30 Gbit/s	0.2 km	NA	3	Sim.
[32]	PAM4	4 × 100 Gbit/s	1.2 m	1540 nm	2	Exp.
This work	DDPD-O-OFDM	48 × 2 × 30.8 Gbit/s	2 m	1528 to 1565.5 nm	1.75 per polarization	Exp.

[30]. Recently reported 8-ary orbital angular momentum (OAM) shift-keying technique not only shows improved tolerance to noise and phase distortions by atmospheric turbulence, but also achieves good spectral efficiency [31]. Besides, a 4 × 100 Gbit/s 4-level pulse amplitude modulation (PAM4) FSOC system is reported achieving a spectral efficiency of 2 and free-space transmission of 1.2 m.

In this work, we put forward and provide the first illustration up to our knowledge of a high capacity and high spectral efficient FSOC system using digital domain power division multiplexing OFDM (DDPD-O-OFDM) signal utilizing 10-GHz class optical components. In the proof-of-concept demonstration, a net data rate of 2 × 30.8 Gbit/s can be achieved for each polarization multiplexed DDPD-O-OFDM wavelength channel, fulfilling the pre-forward-error-correction bit-error-ratio (pre-FEC BER = 3.8 × 10⁻³). The 10-GHz class optical components are optimized for the 10G-PON systems, allowing seamless integration of the typical fiber access and FSOC [33]. Here, the DDPD-O-OFDM is inspired by the works [34], [35], which is generally used for multiple access by different users. The DDPD-O-OFDM can be considered as a case of single-user non-orthogonal multiple access (NOMA) [36]–[38] consuming all the multiplexed data capacity using the SIC process inside a single user Rx. By employing the DDPD-O-OFDM here, the

FSOC per channel capacity can be enhanced not only allowing the spectral overlapping of different orthogonal subcarriers, as in the case of OFDM; but also allowing channel multiplexing in the power domain to increase the spectral efficiency. As different DDPD channels are digitally multiplexed in power domain with superposition coding, successive interference cancellation (SIC) is employ to demultiplex different DDPD channels. The principle of DDPD-O-OFDM is discussed; and BER and signal-to-noise ratio (SNR) of different DDPD channels are experimentally measured.

II. DDPD-O-OFDM PRINCIPLE AND ALGORITHMS

This section will discuss the principle of DDPD-O-OFDM. We assume that the input signal x is divided into different DDPD data signals x_i. The corresponding power for each DDPD data signal is P_i, where i represents how many divided signals. Hence, the input data can be expressed in (1).

$$x = \sum_i \sqrt{P_i} x_i \qquad (1)$$

In this work, we use two DDPD data signal; hence, Eq. (1) can be expressed as (2).

$$x = \sqrt{P_1} x_1 + \sqrt{P_2} x_2 \qquad (2)$$

Here, we study the indoor channel characteristics for the VLC system. The channel response of the FSOC system with multiple-bounce power spectral distribution (PSD) [39] can be expressed in (3),

$$h(t) = \sum_{k=0}^{\infty} h^{(k)}(t; \Phi_n) \qquad (3)$$

where Φ_n is the PSD of different light sources. The response after k-bounces is described in (4),

$$h^{(k)}(t; \Phi_n) = \int_S \left[L_1 \ldots L_{k+1} \Gamma_n^{(k)} rect\left(\frac{\theta_{k+1}}{FOV}\right) \cdot \right.$$
$$\left. \delta\left(t - \frac{d_1 + \ldots + d_{k+1}}{c}\right) \right] dA_{ref} \qquad (4)$$

where

$$L_1 = \frac{A_{ref}(m+1)\cos^m \phi_1 \cos \theta_1}{2\pi d_1^2}, \cdots,$$
$$L_{k+1} = \frac{A_{PD} \cos \phi_{k+1} \cos \theta_{k+1}}{\pi d_{k+1}^2}, \qquad (5)$$

represent the path-loss terms in each path. S is the surface of reflectors, c is the speed of light, A_{ref} is the area of reflecting element. The angles of irradiance and incidence are ϕ_k and θ_k respectively. The received power is inversely proportional to the square of distance d_k. The $\Gamma_n^{(k)}$ represents the power of reflected ray after k-bounces from the light source. The photodiode (PD) can receive optical signal with angle of incidence smaller than the field-of-view (FOV) of PD, as shown in (6).

$$rect(x) = \begin{cases} 1 \ for \ |x| \le 1, \\ 0 \ for \ |x| > 1. \end{cases} \qquad (6)$$

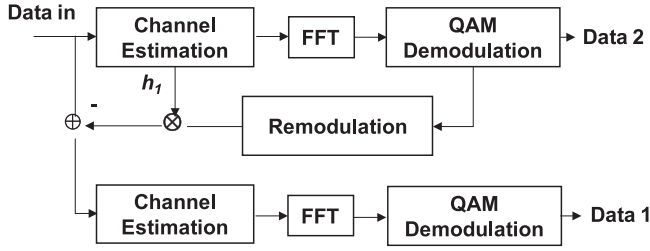Fig. 1. The algorithm of successive interference cancelation (SIC) process.

III. EXPERIMENT

Fig. 2 shows the experiment of the proposed DDPD-O-OFDM FSOC system. The input data will be divided into Data-1 and Data-2, which are then mapped into quadrature amplitude modulation (QAM) format to construct the DDPD-O-OFDM signal. The QAM format used is quadrature-phase-shift-keying (QPSK). Then the data are allocated into different OFDM sub-carriers. After this, the two data channels at different power levels are super-positioned in the digital domain to produce the DDPD-O-OFDM signal using MATLAB program. The power levels of different data channel shape the constellation diagrams. This can be implemented by multiplying each data by a specified power level P_1 and P_2. After that, the OFDM encoding procedure can be employed, including inverted fast-Fourier transform (IFFT), parallel-to-serial conversion (P/S) and cyclic prefix (CP) insertion. In the experiment, the FFT size, subcarrier number, and CP are 512, 225, and 32 respectively.

As our experiment is in line-of-sight (LOS), (4) can be simplified as (7):

$$h^{(0)}(t; \Phi_n) = L_0 P_n rect\left(\frac{\theta_0}{FOV}\right)\delta\left(t - \frac{d_0}{c}\right) \quad (7)$$

where

$$L_0 = \frac{A_{PD}(m+1)\cos^m \phi_0 \cos \theta_0}{2\pi d_0^2} \quad (8)$$

The received signal is shown in (9), where the h_i and n_i are the channel response and noises respectively.

$$y_i = h_i x_i + n_i \quad (9)$$

As shown in (2), different DDPD data signals should preserve a certain power ratio for the successful demodulation. In order to successfully recover the transmitted DDPD data, zero-forcing (ZF) is performed using basic channel inversion as shown as (10).

$$z_i = x_i + h_i^{-1} n_i \quad (10)$$

The SIC is also needed following the order of increasing channel gain. In this experiment, Data-2 has a higher power than Data-1 (i.e., $P_2 > P_1$); hence, Data-2 can be directly decoded without the need of SIC process. This is because Data-1 is treated as a noise due to much lower power. After this, re-modulation of Data-2 is needed in order to extract Data-1. Fig. 1 shows the algorithm of the SIC process used in this work. In order to extract Data-1, the channel response h_1 is needed and it can be obtained after decoding the Data-2. It is also worth to mention that if more DDPD data channels are used, the SIC process shown in Fig. 1 can be repeated by decoding the highest power DDPD data channel first, followed by lower power DDPD data channels. The Data-1 and Data-2 are digitally combined using MATLAB program at the transmitter (Tx), they have the same bandwidth BW and a noise power P_N. (11) shows that the total capacity C is equal to the summation of capacities of all DDPD data channels, where the capacity C_2 from Data-2 is limited by the transmission noise P_N together with the interference noise from Data-1. On the other hand, the capacity C_1 is only limited by P_N only.

$$\begin{aligned} C &= C_2 + C_1 \\ &= BW\log_2\left(1 + \frac{|h_2|^2 P_2}{|h_1|^2 P_1 + P_N}\right) + BW\log_2\left(1 + \frac{|h_1|^2 P_1}{P_N}\right) \end{aligned} \quad (11)$$

The DDPD-O-OFDM signal generated digitally in the MAT-LAB program is then stored in a digital-to-analog converter (DAC), which is used to transform the digital DDPD-O-OFDM signal into real electrical waveforms. In this experiment, the DAC is an arbitrary waveform generator (AWG, Tektronix AWG 70001) with 50 GS/s sampling rate and 20 GHz analog bandwidth. The C-band optical signals produced by different distributed feedback (DFB) LDs are modulated by the DDPD-O-OFDM signal emitted by the AWG via 10-GHz class Mach-Zehnder modulators (MZMs). Polarization multiplexing and demultiplexing of each wavelength channel are performed via polarization beam combiner (PBC) / polarization beam splitter (PBS). All the C-band wavelength channels are combined and amplified by a wavelength multiplexer and an EDFA respectively, before being launched to the receiver (Rx) via a 2-m free-space transmission link. A pair of C-band optical collimators are used at the Tx and Rx sides. They are mounted on translation stages with 6 degrees of freedoms as shown in the insets of Fig. 2.

At the Rx side, the C-band wavelength channels are wavelength demultiplexed. A variable optical attenuator (VOA) is used to adjust the received optical power for the BER analysis. Then polarization demultiplexing is performed at each wavelength channel before received by 10-GHz PDs. The DDPD-O-OFDM signal received by each PD is captured by a real time scope (RTO, LeCroy 816ZI-B) which has an analog bandwidth of 16 GHz and sampling rate of 80 GSample/s. The RTO act as the analog-to-digital converter (ADC) transforming the captured DDPD-O-OFDM waveforms into digital domain for the power domain demultiplexing and OFDM decoding. The digital decoding is performed using LabVIEW and Matlab programs. The demodulation process of the DDPD-O-OFDM signal include the data serial-to-parallel (S/P) conversion, zero forcing implementation, and channel estimation, which is needed to de-multiplex DDPD-O-OFDM data channels as discussed in Section II. In this proof-of-concept demonstration, the SIC process discussed in Section II is used to retrieve the different DDPD data channels. The first step is to estimate the gain from the channel response to decide the decoding sequence. The higher power DDPD channel
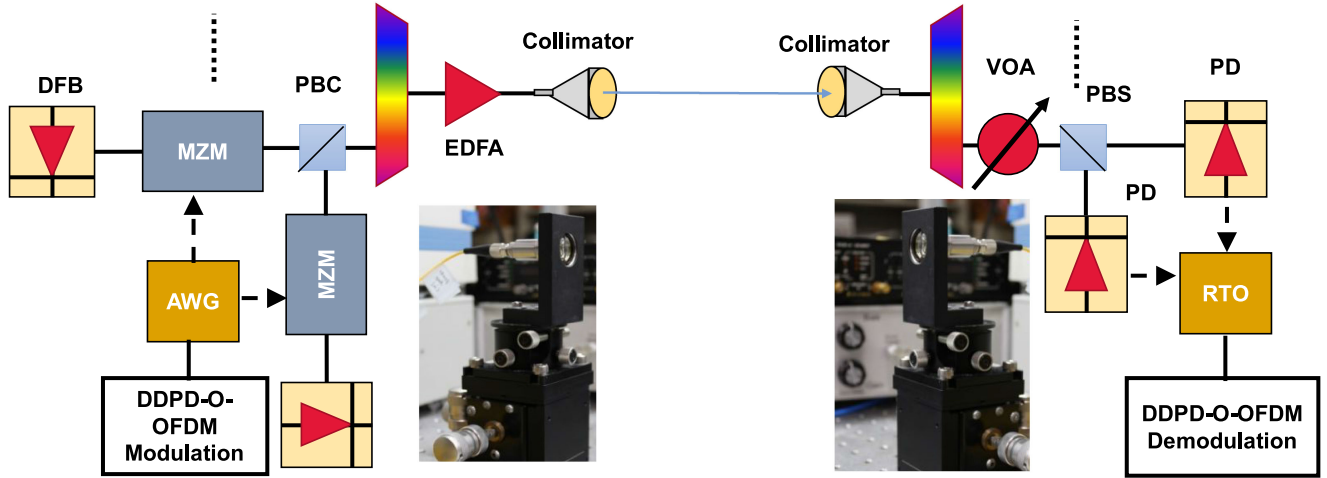
Fig. 2. Experiment of the proposed DDPD-O-OFDM FSOC system. DFB: distributed feedback laser diode; MZM: Mach-Zehnder modulator; AWG: arbitrary waveform generator; PBC: polarization beam combiner; EDFA: erbium-doped fiber amplifier; VOA: variable optical attenuator; PBS: polarization beam splitter; PD: photodiode; RTO: real time oscilloscope.
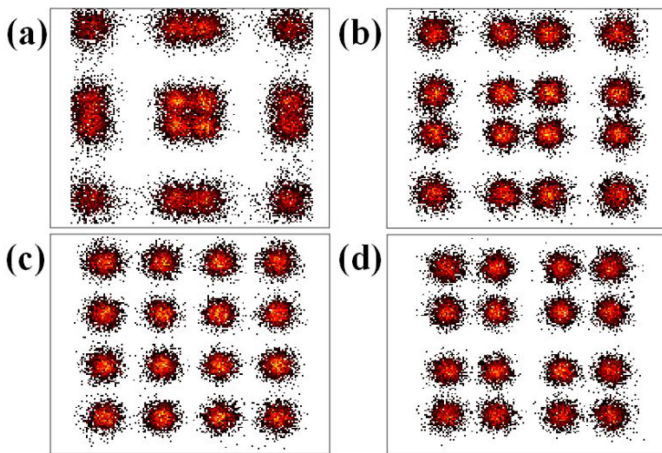

Fig. 3. Experimental DDPD-O-OFDM constellation diagrams with power ratios of (a) 1:2, (b) 1:3, (c) 1:4, and (d) 1:5.

is decoded first, while considering other signals as noises. In this experiment, Data-2 has the highest power, and it is decoded first while Data-1 is treated as noise. The second step is to re-modulate the estimate signal and multiply it by the channel response h_1 before subtracting it from the total DDPD-O-OFDM signal. Then, the second channel can be decoded, which is Data-1.

IV. RESULTS AND DISCUSSION

As discussed before, the two data channels are enfolded in power domain, and their constellation are shaped based on their power distribution. A proper power ratio should be maintained between the two data channel to maximize the system capacity and at the same time to satisfy the pre-FEC BER requirement. In this experiment, originally both the Data-1 and Data-2 utilize 4-QAM (QPSK) format. Since these two data channels are superimposed with power division multiplexing as illustrated
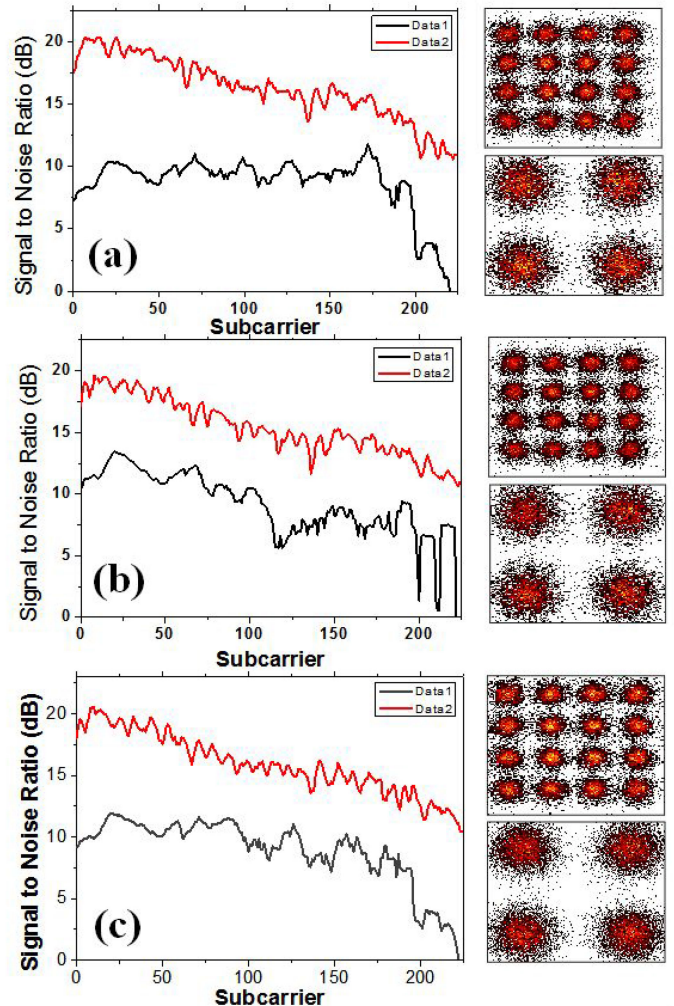

Fig. 4. Experimental SNRs of the Data-1 and Data-2 over all the 225 OFDM subcarriers for the wavelength channels at (a) 1530 nm, (b) 1540 nm, and (c) 1550 nm.
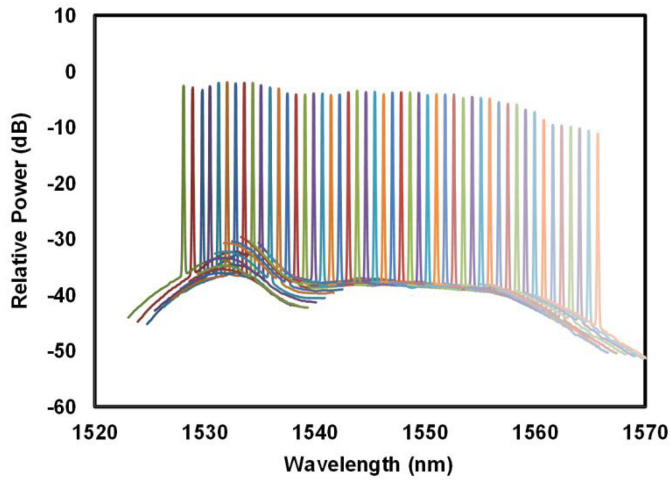
Fig. 5. Measured optical spectra of the 48 DDPD-O-OFDM wavelength channels over the wavelength range from 1530 nm to 1560 nm.
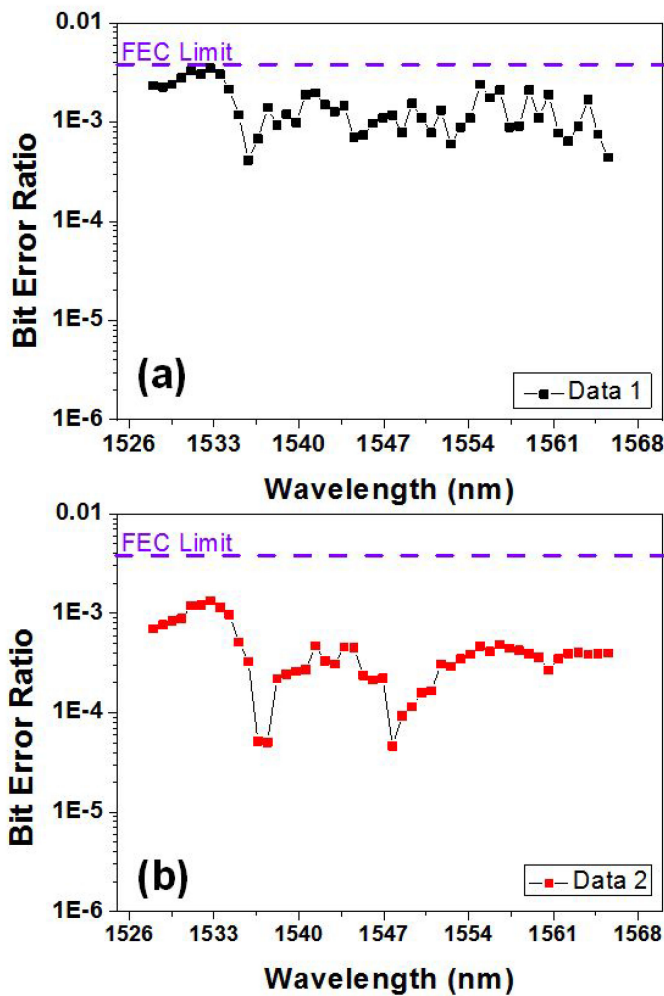

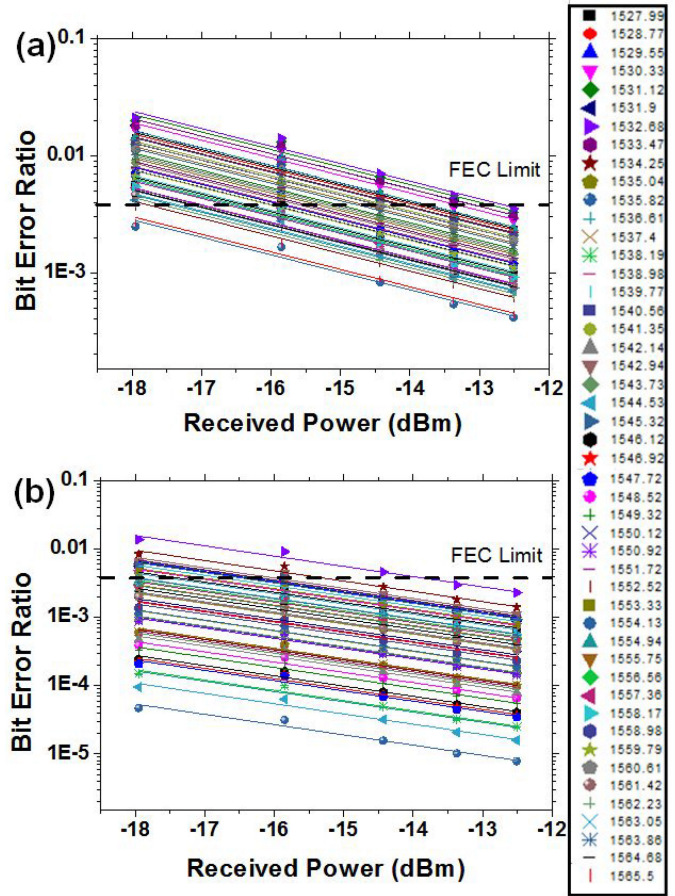Fig. 7. Measured BER curves of (a) Data-1 and (b) Data-2 in different DDPD-O-OFDM wavelength channels.

Fig. 6. Measured BER characteristics of (a) Data-1 and (b) Data-2 in different DDPD-O-OFDM wavelength channels.

in Eq. (2), the constellation of DDPD-O-OFDM signal looks like 16-QAM before the SIC. Figs. 3(a)-(d) illustrate the experimental DDPD-O-OFDM constellation diagrams using different power ratios applied on the system. We can observe that the constellation diagram looks differently at different power ratios. Based on our analysis, the power ratio of Data-1:Data-2 of 1:4 provides the optimum performance for both DDPD channels; hence, this power ratio is selected in subsequent experiment as shown in Fig. 3(c).

We arbitrarily selected 3 different wavelengths at 1530 nm, 1540 nm, and 1550 nm out of the 48 wavelengths to illustrate the SNRs of the DDPD-O-OFDM signals at different parts of the C-band spectrum. Besides, the constellation diagrams before and after the SIC process are also included. Fig. 4(a) shows the SNRs of the 1530 nm wavelength channel. The average SNRs for Data-1 and Data-2 are 7.36 dB and 15.47 dB respectively, and the corresponding BERs are 2.79×10^{-3} and 7.5×10^{-4} respectively. Fig. 4(b) shows the SNRs of the 1540 nm wavelength channel. The average SNRs for Data-1 and Data-2 are 8.3 dB and 15.24 dB respectively, and the corresponding BERs are 1.89×10^{-3} and 1.5×10^{-4} respectively. Moreover, Fig. 4(c) shows the SNRs of the 1550 nm wavelength channel. The average SNRs for Data-1 and Data-2 are 11.96 dB and 16.02 dB, and the BERs are 1.1×10^{-3} and 2.76×10^{-4} respectively.

Fig. 5 presents the measured optical spectra of the 48 DDPD-O-OFDM wavelength channels over the wavelength range from 1530 to 1560 nm. It is measured by an optical spectrum analyzer (OSA) having resolution of 0.03 nm, video bandwidth of 10 Hz. Fig. 6(a) and (b) show the Data-1 and Data-2 BER characteristics of different DDPD-O-OFDM wavelength channels.

In this proof-of-concept demonstration, a net data rate of 30.8 Gbit/s in each polarization can be achieved by considering the CP and the 7% FEC. Hence, 2×30.8 Gbit/s can be achieved in both polarizations. Here, 48 wavelengths at C-band are employed achieving a total FSOC capacity of 2.957 Tbit/s. By considering the optical signal bandwidth of 17.6 GHz [40], the calculated spectral efficiency is 30.8 Gbit/s / 17.6 GHz = 1.75 bit/s/Hz per polarization. Fig. 7(a) and (b) show the measured BER curves of all the DDPD-O-OFDM wavelength channels. The BER measurement is performed by first selecting a specific DDPD-O-OFDM wavelength channel, then the whole signal waveform is captured at different received optical power adjusted by the VOA. After this, the BER of Data-2 is obtained by decoding the DDPD-O-OFDM signal. Finally, the SIC process is executed to obtain the BER of Data-1. It is worth to note that we have to maintain a fix power ratio between Data-1 and Data-2 for all the wavelength channels. Hence, we can observe that although both Data-1 and Data-2 can satisfy the pre-FEC requirement, the obtained BERs for both Data-1 and Data-2 are different. As shown in Fig. 7(a) and (b), all the DDPD-O-OFDM wavelength channels in the C-band can satisfy the pre-FEC BER when the received optical power is larger than -12.5 dBm.

V. CONCLUSION

Although the cost of optical fiber is low, underground installation is costly and time consuming. The concept of combining fiber access and FSOC has been proposed recently. FSOC can provide many transmission advantages. In this work, we put forward and provided the first illustration of a high capacity and high spectral efficient FSOC system using DDPD-O-OFDM signal utilizing 10-GHz class optical components. In the proof-of-concept demonstration, a net data rate of 2×30.8 Gbit/s can be achieved for each polarization multiplexed DDPD-O-OFDM wavelength channel. Here, the principle of DDPD-O-OFDM was discussed. Experimental results revealed that all the 48 DDPD-O-OFDM wavelength channels in the C-band can satisfy the pre-FEC BER when the received optical power was greater than -12.5 dBm; and a total FSOC capacity of 2.957 Tbit/s were achieved.

REFERENCES

[1] L. Y. Chan, C. K. Chan, D. T. K. Tong, F. Tong, and L. K. Chen, "Upstream traffic transmitter using injection-locked Fabry-Pérot laser diode as modulator for WDM access networks," *Electron. Lett.*, vol. 38, no. 1, pp. 43–45, 2002.

[2] G. Talli and P. D. Townsend, "Hybrid DWDM-TDM long-reach PON for next-generation optical access," *J. Lightw. Technol.*, vol. 24, no. 7, pp. 2827–2834, Jul. 2006.

[3] L. Zhou, H. He, Y. Zhang, Y. Chen, Q. Xiao, and Z. Dong, "Enhancement of spectral efficiency and power budget in WDN-PON employing LDPC-coded probabilistic shaping PAM8," *IEEE Access*, vol. 8, pp. 45 766–45 773, 2020.

[4] M. Bi *et al.*, "Power budget improvement of symmetric 40-Gb/s DML-based TWDM-PON system," *Opt. Exp.*, vol. 22, pp. 6925–6933, 2014.

[5] C. W. Chow, C. H. Yeh, C. H. Wang, F. Y. Shih, C. L. Pan, and S. Chi, "WDM extended reach passive optical networks using OFDM-QAM," *Opt. Exp.*, vol. 16, pp. 12 096–12 101, 2008.

[6] W. Y. Lin *et al.*, "A hybrid CATV/OFDM long-reach passive optical network architecture," *Opt. Exp.*, vol. 20, pp. 4219–4224, 2012.

[7] J. Zhou *et al.*, "8 × 10 Gb/s downstream PAM-4 transmission for cost-effective coherent WDM-PON application," *J. Lightw. Technol.*, vol. 39, no. 9, pp. 2837–2846, Sep. 2021.

[8] S. T. Hayle *et al.*, "Integration of fiber and FSO network with fault-protection for optical access network," *Opt. Commun.*, vol. 484, 2021, Art. no. 126676.

[9] C. H. Yeh, B. S. Guo, C. S. Gu, C. W. Chow, and W. P. Lin, "Use of same WDM channels in fiber network for bidirectional free space optical communication with Rayleigh backscattering interference alleviation," *IEEE Access*, vol. 7, pp. 169571–169576, 2019.

[10] C. H. Yeh, J. R. Chen, W. Y. You, and C. W. Chow, "Hybrid WDM FSO fiber access network with Rayleigh backscattering noise mitigation," *IEEE Access*, vol. 8, pp. 96449–96454, 2020.

[11] C. L. Ying, H. H. Lu, C. Y. Li, C. A. Chu, T. C. Lu, and P. C. Peng, "A bidirectional hybrid lightwave transport system based on fiber-IVLLC and fiber-VLLC convergences," *IEEE Photon. J.*, vol. 7, no. 4, Apr. 2015, Art. no. 7201611.

[12] H. W. Wu, C. Y. Li, H. H. Lu, Q. P. Huang, S. C. Tu, and Y. C. Huang, "A PDM-based 128-Gb/s PAM4 fibre-FSO convergent system with OBPFs for polarisation de-multiplexing," *Sci. Rep.*, vol. 10, 2020, Art. no. 1872.

[13] C. W. Chow *et al.*, "Enabling techniques for optical wireless communication systems," in *Proc. Opt. Fiber Commun. Conf. Exhib.*, 2020, pp. 1–3.

[14] H. Haas, "LiFi is a paradigm-shifting 5G technology," *Rev. Phys.*, vol. 3, pp. 26–31, 2018.

[15] C. W. Chow, C. H. Yeh, Y. F. Liu, and Y. Liu, "Improved modulation speed of LED visible light communication system integrated to main electricity network," *Electron. Lett.*, vol. 47, pp. 867–868, 2011.

[16] H. L. Minh *et al.*, "100-Mb/s NRZ visible light communications using a post-equalized white LED," *IEEE Photon. Technol. Lett.*, vol. 21, no. 15, pp. 1063–1065, Aug. 2009.

[17] L. Y. Wei, C. W. Chow, G. H. Chen, Y. Liu, C. H. Yeh, and C. W. Hsu, "Tricolor visible-light laser diodes based visible light communication operated at 40.665 Gbit/s and 2 m free-space transmission," *Opt. Exp.*, vol. 27, pp. 25072–25077, 2019.

[18] N. Chi, Y. Zhou, Y. Wei, and F. Hu, "Visible light communication in 6G: Advances, challenges, and prospects," *IEEE Veh. Technol. Mag.*, vol. 15, no. 4, pp. 93–102, Dec. 2020.

[19] S. A. Al-Gailani *et al.*, "A survey of free space optics (FSO) communication systems, links, and networks," *IEEE Access*, vol. 9, pp. 7353–7373, 2021.

[20] M. Ijaz *et al.*, "Experimental investigation of the performance of different modulation techniques under controlled FSO turbulence channel," in *Proc. 5th Int. Symp. Telecommun.*, 2010, pp. 59–64, doi: 10.1109/IS-TEL.2010.5733999.

[21] S. A. Al-Gailani, A. B. Mohammad, R. Q. Shaddad, U. U. Sheikh, and M. A. Elmagzoub, "Hybrid WDM/multibeam free-space optics for multi-gigabit access network," *Photonic Netw. Commun.*, vol. 29, pp. 138–145, 2015.

[22] J. A. R. P. de Carvalho, H. Veiga, P. A. J. Gomes, C. F. F. P. R. Pacheco, and A. D. Reis, "Experimental performance study of a very high speed free space optics link at the university of beira interior campus: A case study," in *Proc. IEEE Int. Symp. Signal Process. Inf. Technol.*, 2008, pp. 154–157.

[23] F. A. Wahab *et al.*, "Multiple transmitters & receivers for free space optical communication link performance analysis," *J. Telecommun. Electron. Comput. Eng.*, vol. 8, pp. 29–32, 2016.

[24] M. T. Nguyen, V. Mai, and H. Kim, "Multiple-aperture direct-detection receiver based on maximal ratio combining for FSO communication," *IEEE Photon. Technol. Lett.*, vol. 34, no. 8, pp. 405–408, Apr. 2022.

[25] J. Singh and N. Kumar, "Performance analysis of different modulation format on free space optical communication system," *Optik*, vol. 124, pp. 4651–4654, Oct. 2013.

[26] N. Badar and R. K. Jha, "Performance comparison of various modulation schemes over free space optical (FSO) link employing gamma–gamma fading model," *Opt. Quantum Electron.*, vol. 49, 2017, Art. no. 192.

[27] G. Parca, A. Shahpari, V. Carrozzo, G. M. T. Beleffi, and A. L. J. Teixeira, " Optical wireless transmission at 1.6-Tbit/s (16 × 100 Gbit/s) for next-generation convergent urban infrastructures," *Opt. Eng.*, vol. 52, pp. 1161021–1161025, 2013.

[28] V. Sharma and G. Kaur, "High speed, long reach OFDM-FSO transmission link incorporating OSSB and OTSB schemes," *Optik*, vol. 124, pp. 6111–6114, 2013.

[29] K. Kiasaleh, "Performance of APD-based PPM free-space optical communication systems in atmospheric turbulence," *IEEE Trans. Commun.*, vol. 53, no. 9, pp. 1455–1461, Sep. 2005.

[30] H. Liu, R. Liao, Z. Wei, Z. Hou, and Y. Qiao, "BER analysis of a hybrid modulation scheme based on PPM and MSK subcarrier intensity modulation," *IEEE Photon. J.*, vol. 7, no. 4, Aug. 2015, Art. no. 7201510.

[31] A. Munkhbayar, H. Kishikawa, and N. Goto, "8-ary OAM shift keying for FSO link with atmospheric turbulence," in *Proc. OSA Adv. Photon. Congr.*, 2019, Paper SpTh3E.6.

[32] R. Zhang *et al.*, "4 × 100-Gb/s PAM-4 FSO transmission based on polarization modulation and direct detection," *IEEE Photon. Technol. Lett.*, vol. 31, no. 10, pp. 755–758, Oct. 2019.

[33] Z. Hu *et al.*, "Experimental demonstration of 111.1-Gb/s net information rate using IM/DD probabilistically shaped orthogonal chirp-division multiplexing with a 10-GHz-class modulator," *Opt. Exp.*, vol. 27, pp. 33789–33798, 2019.

[34] Z. Feng *et al.*, "Digital domain power division multiplexing DDO-OFDM transmission with successive interference cancellation," in *Proc. Conf. Lasers Electro-Opt.*, 2016, pp. 1–2.

[35] K. Higuchi and A. Benjebbour, "Non-orthogonal multiple access (NOMA) with successive interference cancellation for future radio access," *IEICE Trans. Commun.*, vol. E98.B, no. 3, pp. 403–414, 2015.

[36] W. H. Gunawan, Y. H. Chang, C. W. Chow, Y. Liu, and C. H. Yeh, "High speed RGB visible light communication (VLC) using digital power-domain multiplexing (DPDM) of orthogonal frequency division multiplexed (OFDM) signals," in *Proc. Opt. Fiber Commun. Conf. Exhib.*, 2022, pp. 1–3.

[37] A. Dhariwal, "Performance evaluation of energy efficiency and spectral efficiency: NOMA vs OFDMA," *Telecomm. Syst. Manage.*, vol. 9, 2020, Art. no. 3.

[38] W. U. Khan, J. Liu, F. Jameel, V. Sharma, R. Jäntti, and Z. Han, "Spectral efficiency optimization for next generation NOMA-enabled IoT networks," *IEEE Trans. Veh. Technol.*, vol. 69, no. 12, pp. 15284–15297, Dec. 2020.

[39] K. Lee, H. Park, and J. R. Barry, "Indoor channel characteristics for visible light communications," *IEEE Commun. Lett.*, vol. 15, no. 2, pp. 217–219, Feb. 2011.

[40] D. Tsonev, S. Videv, and H. Haas, "Unlocking spectral efficiency in intensity modulation and direct detection systems," *IEEE J. Sel. Areas Commun.*, vol. 33, no. 9, pp. 1758–1770, Sep. 2015.